Metamaterials-Based Label-Free Nanosensor for Conformation and Affinity Biosensing

Cuong Cao,[†] Jun Zhang,[†] Xinglin Wen,[†] Stephanie L. Dodson,[†] Nguyen Thuan Dao,[†] Lai Mun Wong,[‡] Shijie Wang,[‡] Shuzhou Li,[§] Anh Tuân Phan,[†] and Qihua Xiong[†,⊥,*]

[†]Division of Physics and Applied Physics, School of Physical and Mathematical Sciences, Nanyang Technological University, Singapore 637371, [‡]Institute of Materials Research & Engineering, Agency for Science, Technologies and Research, 3 Research Link, Singapore 117602, [§]Division of Materials Sciences, School of Materials Science and Engineering, Nanyang Technological University, Singapore 639798, and [⊥]NOVITAS, Nanoelectronics Center of Excellence, School of Electrical and Electronic Engineering, Nanyang Technological University, Singapore 639798

ABSTRACT Analysis of molecular interaction and conformational dynamics of biomolecules is of paramount importance in understanding their vital functions in complex biological systems, disease detection, and new drug development. Plasmonic biosensors based upon surface plasmon resonance and localized surface plasmon resonance have become the predominant workhorse for detecting accumulated biomass caused by molecular binding events. However, unlike surface-enhanced Raman spectroscopy (SERS), the plasmonic biosensors indeed are not suitable tools to interrogate vibrational signatures of conformational transitions required for biomolecules to interact. Here, we show that highly tunable plasmonic metamaterials can offer two transducing channels for parallel acquisition of optical transmission and sensitive SERS spectra at the biointerface, simultaneously probing the conformational states and binding affinity of biomolecules, *e.g.*, G-quadruplexes, in different environments. We further demonstrate the use of the metamaterials for fingerprinting and detection of the arginine-glycine-glycine domain of nucleolin, a cancer biomarker that specifically binds to a G-quadruplex, with the picomolar sensitivity.

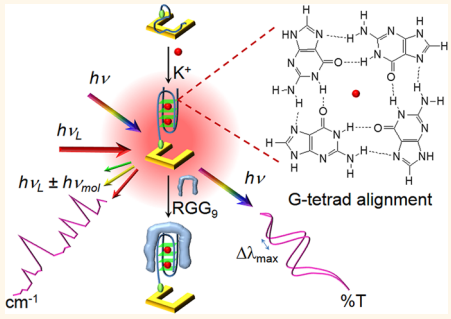

KEYWORDS: metamaterials · biosensor · G-quadruplex DNA · conformation analysis · surface-enhanced Raman spectroscopy · refractive index sensing · localized surface plasmon resonance

The basis of life-sustaining activities relies on accurate folding and binding of biomolecules.[1] Comprehensive understanding of conformational states, expressions, and binding processes of the biomolecules will thus significantly impact a myriad of fields including genomic research, functional proteomics, clinical diagnosis, disease treatment, and new drug development. Label-free surface plasmon resonance (SPR) and localized surface plasmon resonance (LSPR) biosensors have been developed to increase our knowledge in this regard.[2−5] Despite the undisputed strength in providing quantitative information, binding affinity, and kinetic rate from molecules that change the local refractive index, they are not well-suited to provide information regarding conformations or chemical fingerprints of unknown molecules.[3] In contrast, plasmonic biosensors based upon surface-enhanced Raman scattering (SERS) can interrogate vibrational signatures of conformational transitions.[6,7] However, one of the major concerns in SERS-based biosensing is the problem with poor reproducibility and controllability of the conventional SERS-active substrates (*e.g.*, nanoparticles).[8,9] In addition, by its enhancement mechanism the SERS intensity is highly dependent on proximity and orientation of the biomolecules with respect to the metal surface. Therefore, SERS-based biosensing usually suffers from a wide distribution of enhancement factors, thus lacking reliably quantifiable signals.[8,9] Therefore, multichannel and label-free devices targeted for both quantitative and qualitative assessments that could significantly contribute to the fields of structural biology and analytical sciences are demanded.

Recently, metamaterials have emerged as an excellent sensing technology that complements traditional plasmonic biosensors based on metallic colloidal nanoparticles or

* Address correspondence to Qihua@ntu.edu.sg.

Received for review April 3, 2013 and accepted August 17, 2013.

Published online August 17, 2013
10.1021/nn401645t

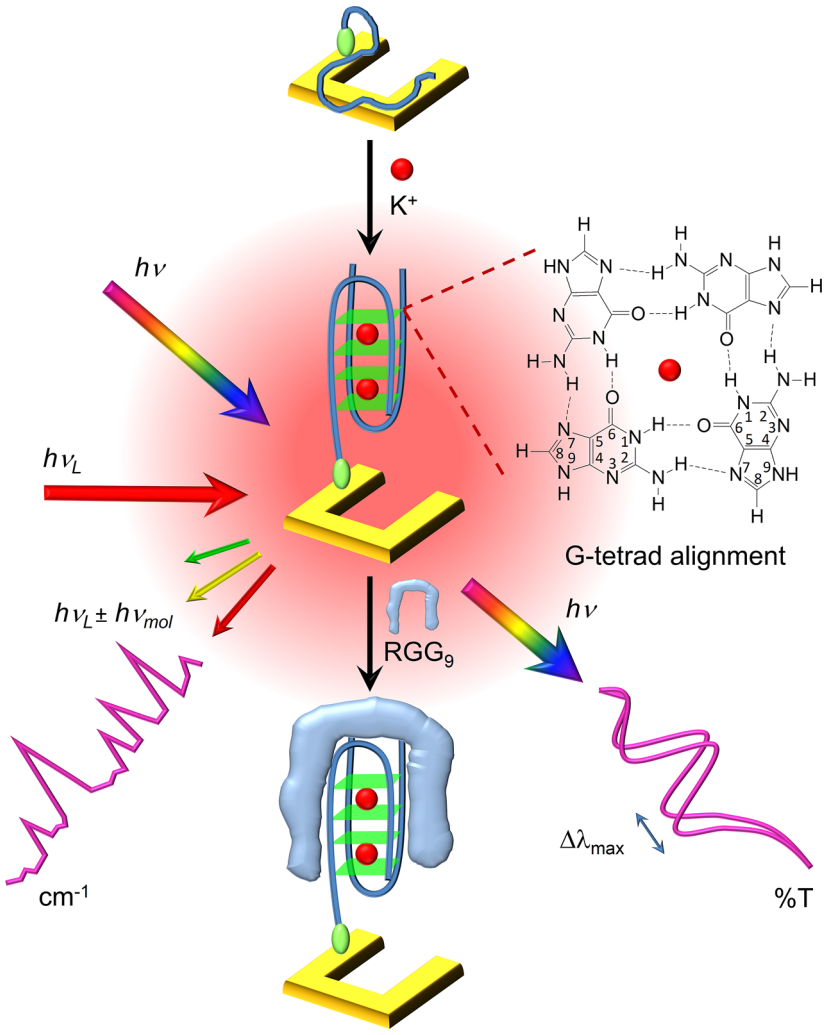

Figure 1. Schematic illustration of vis−NIR SRR metamaterials as a dual transducing mode nanosensor for the detection and identification of biomolecules. Designed to operate in the vis−NIR region of the electromagnetic spectrum, the plasmonic metamaterials will provide direct access to characteristic fingerprints of biomolecules, thus enabling a unique platform to execute both conformational information and quantitative binding data simultaneously by transmission and SERS spectroscopies. The SRR nanosensor is functionalized with AS1411, an effective anticancer drug that is currently in clinical trials for cancer treatment. Under K^+-induced conditions, AS1411 folds into a G-quadruplex, which can effectively capture the RGG_9 binding region of a nucleolin biomarker.

nanostructures.[10−14] Metamaterials are large-scale, densely packed periodic "artificial atoms", *i.e.*, split-ring resonators (SRRs), whose optical properties go beyond the limitations of conventional, naturally occurring optical materials or composites.[15−17] By engineering the SRRs' geometry, one can independently control their electronic and magnetic responses from microwave to terahertz regimes.[16,18] Especially, the plasmonic responses of metamaterials can be tuned to the visible−near-infrared (vis−NIR) region of the electromagnetic spectrum,[19,20] which is in resonance with available laser frequencies widely used in spectroscopy, enabling a strong signal enhancement for both quantitative measurement and molecular identification. For instance, tuning of the metamaterial resonances to specific vibrational modes of a chemical or biological molecule has been demonstrated for fingerprinting and detection of small organic molecules (*e.g.*, *p*-mercaptoaniline,[13] octadecanthiol[21]), DNA,[10] and proteins.[11,14,22] However, capabilities in resolving primary and secondary structures, conformational dynamics, and binding affinity of complex biological systems still remain to be addressed.

Here, we show that a tunable vis−NIR metamaterials-based nanosensor with a complementary nature of dielectric sensing and SERS molecular identification can be realized, thereby improving the specificity of biodetection and providing the basis for label-free conformational resolving and quantitative detection within a single plasmonic platform with picomolar sensitivity. We select a guanine-rich oligonucleotide (GRO), namely, AS1411 (26 mer, 7.8 kDa), as a plasmonic response modulator because of its biophysical and biological significance upon conformation change. In the presence of monovalent ions such as K^+ or Na^+, single-stranded AS1411 oligonucelotides fold into four-stranded G-quadruplexes *via* Hoogsteen hydrogen-bonded G-tetrad (or G-quartet) squares (Figure 1).[23] The transition from unfolded to folded state of the G-quadruplex results in a

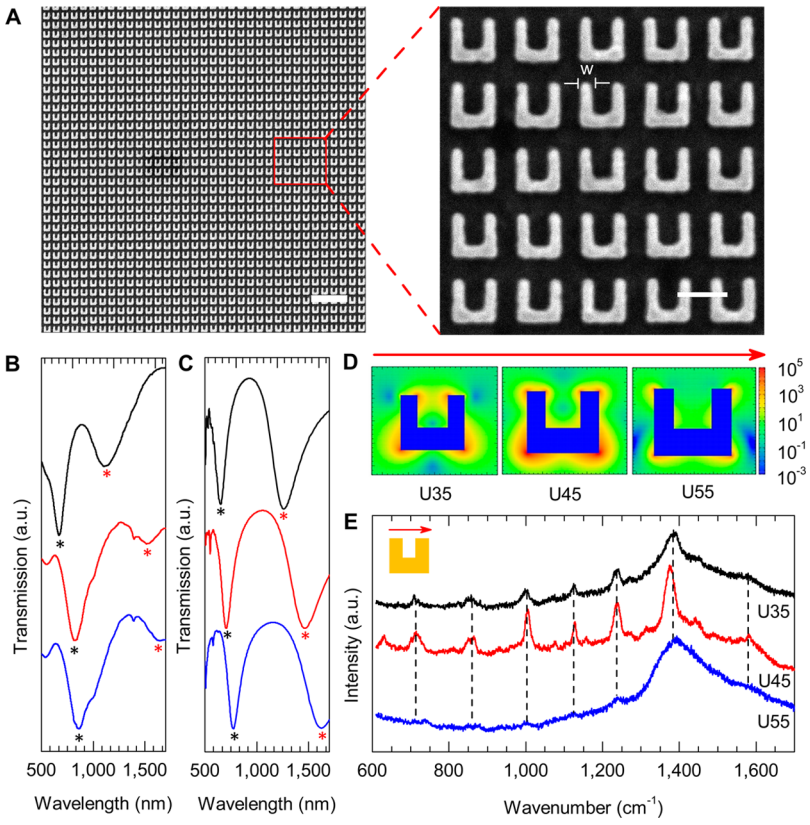

Figure 2. Fabrication and characterization of SRRs. (A) Representative SEM micrographs of U45 SRRs with average width w = 45.2 ± 2.6 nm measured from 20 structures (from left to right, the scale bars are 1 μm and 200 nm, respectively). Transmission spectra of the U35 (black curves), U45 (red curves), and U55 SRRs (blue curves) from experimental measurements (B) and theory calculation by finite difference time-domain (FDTD) (C). The ER and MR modes are marked with black and red asterisks, respectively. (D) Simulation of electromagnetic field enhancement for three different sized SRRs using the DDA method. The simulation is performed at excitation wavelength of 785 nm; the E-field polarization is parallel to the gap. (E) Experimental Raman spectra of the SRRs attached to 10 μM thiolated AS1411. The U45 SRRs generate the strongest Raman signal, which agrees well with the simulation result.

distinct structural and chemical nature that can consequently be detected and identified by transmission and Raman scattering spectroscopy using metamaterials. Furthermore, when the G-quadruplex DNA is formed, it can tightly bind to proteins such as nucleolin, the most abundant nucleolar phosphoprotein in the nucleus of all eukaryotic cells and that is often overexpressed at a high level in human cancer cells,[24] *via* RNA binding domains and an arginine-glycine-glycine (RGG_9 peptide) region with high specificity.[25] It has been suggested that the binding of an AS1411 G-quadruplex aptamer interferes with the normal functions of nucleolin and strongly inhibits cancer cell proliferation, enabling the AS1411 G-quadruplex to be an effective anticancer drug that is currently in clinical trials for renal cell carcinoma and acute myelogenous leukemia.[24,26] Based on this, G-quadruplex DNA will be used as a capturing element for detection and identification of the RGG_9 domain of nucleolin by the dual-mode SRR nanosensor (Figure 1).

RESULTS AND DISCUSSION

Au U-shaped SRRs with different line widths of ~35, ~45, and ~55 nm (abbreviated U35, U45, and U55) were fabricated by electron beam lithography (see Figure S1 for geometrical parameter and periodicity values). Figure 2A shows the representative SEM images of the U45 SRRs with a uniformity of device width of 45.2 ± 2.6 nm across the arrays. The experimental transmission spectra (Figure 2B) show two resonance peaks located at the visible region and near-infrared region corresponding to electric resonance (ER) and magnetic resonance (MR), respectively. These two modes have been well assigned and discussed in the literature: The ER is due to the collectively charged oscillation of the free conduction electrons within the nanometer-sized metallic structure, and the artificial MR is caused by the molecular loop current when the electric polarization is along the gap-bearing side of SRRs.[17−19,27,28] As the size of the SRRs increases from ~35 to ~55 nm, the resonance modes systematically shift to longer wavelength (Figure 2B), which can be explained using an LC circuit model.[18,19] The finite difference time-domain (FDTD) transmission simulations based on MEEP codes[29] for three different sizes of the U-shaped SRRs are also shown in Figure 2C, indicating a good agreement with the experimental observations. The slight difference in resonance peak position is attributed to the topological deviation between the experiments and the calculations. In addition,

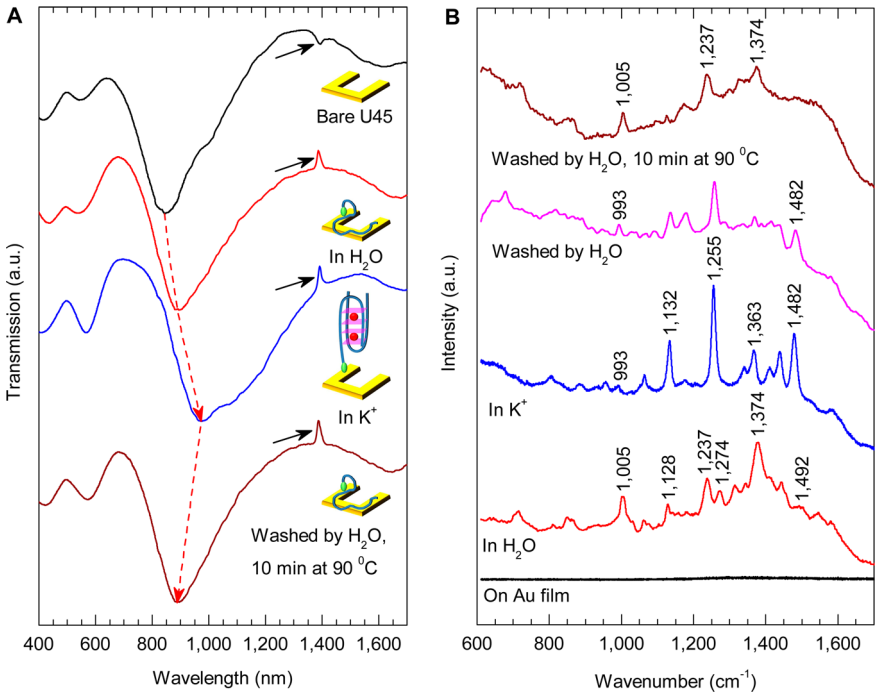

Figure 3. Conformation analysis of G-quadruplex DNA using vis−NIR SRR metamaterials. (A) Vis−NIR analysis of the functionalized SRRs. Electric resonances of the bare U45 SRRs, after immobilization of 10 μM thiolated AS1411, after the thiolated AS1411 folded into a G-quadruplex in K^+ buffer, and after regeneration are 844, 895, 970, and 889 nm, respectively. The black arrows indicate artifact peaks in the spectra caused by the Craic 20 microspectrophotometer. (B) Raman scattering spectroscopy using a U45 SRR surface for the identification of DNA conformation in water and in K^+ buffer.

sensitivity to the refractive index (RI) of the ER mode increases from 137 to 339 nm per refractive index unit (RIU) as the feature size increases. This value is similar to that of conventional LSPR biosensors, of which the sensitivities usually do not exceed 100 to 300 nm per RIU.[3,12,30−32] More interestingly, the MR mode that is not present in natural plasmonic nanostructures was found to be more sensitive to the RI, which increases from 378 to 655 nm per RIU (Figure S2).

Basically, hot spots with high local electromagnetic field intensities are present in any LSPR nanostructures. However, the greatest local field enhancement in SERS is obtained only when the Raman excitation wavelength is close to the resonance frequency of the LSPR nanostructures.[3,33,34] To study the correlation of SERS to the resonance wavelength, a 785 nm diode laser was used as the excitation source with a parallel polarization to the gap of the SRRs. The local electric field $|E|^4$ contour mapping conducted by discrete dipole approximation (DDA)[35−37] indicates that U45 SRRs generate the strongest local field enhancement (Figure 2D). Figure 2E shows that the experimental SERS spectra of the 10 μM thiolated AS1411 DNA attached on the SRRs are consistent with the simulation, in which the SERS spectrum of AS1411 DNA on the U45 SRRs demonstrates the greatest intensity. It should be noted that under the same 785 nm laser excitation no Raman signal for the AS1411 DNA could be obtained in both solution phase and dry state when the SRR substrate is not in use (Figure S3). Therefore, to calculate the electromagnetic enhancement factor (EF), the SRR metamaterials were examined by performing SERS with a covalently self-assembled monolayer of a Raman-active chemical, 2-naphthalenethiol (Figure S4).[38] The ring−ring stretching band at 1380 cm^{-1} of 2-naphthalenethiol was selected to investigate the EF. More details about the EF calculation are presented in the Supporting Information. The EF for the U45 SRRs was found to be $\sim 6.5 \times 10^7$, which is the highest value compared to that of U35 and U55. This EF value is comparable to, or even larger than, those obtained from other SERS nanomaterials for the naphthalenethiol analysis[39,40] and is strong enough to allow a sensitivity of detection down to the single-molecule regime.[8,9] A comprehensive study on the electromagnetic tunability and enhancement will be presented elsewhere. Therefore, the U45 SRR was selected as the substrate for the demonstration in this paper.

Figure 3A displays the transmission spectra of the functionalized SRRs. Respectively, the ER and MR peaks of the U45 SRRs shift from 844 to 895 nm and from 1620 to 1678 nm after the immobilization of 10 μM thiolated AS1411 as the sample was treated in water. As treated with K^+ buffer containing free single-stranded AS1411 (see Methods), the ER mode further red-shifts to 970 nm while the MR mode shifts to over 1700 nm, which is out of the spectral coverage of the Craic 20 microspectrophotometer. The large wavelength shift (~75 nm in ER) corresponds to the refractive index change caused by both (i) the K^+ buffer (generating a shift of ~52 nm; see Figure S5) and (ii) the formation of possible intermolecular G-quadruplex

structures from the single-stranded and unfolded AS1411 DNA. The black arrows point to the spectral artifacts of the microspectrometer. Previously, there has been an attempt to utilize LSPR spectral shifts on silver nanoprisms fabricated by nanosphere lithography for the conformation analysis of calmodulin protein;[4,41] however it was unable to draw any conclusion about the secondary or tertiary conformation changes. In our study, by parallel acquisition of the transmission and SERS from large functionalized SRR arrays, not only the binding adsorptions but also the conformational dynamics and chemical signatures of biomolecules in their natural environment can be revealed. Indeed, a significant difference between unfolded single-stranded AS1411 and the folded AS1411 G-quadruplex was observed by Raman scattering spectroscopy (Figure 3B). As treated in water, the unfolded AS1411 possesses an intense Raman peak at 1005 cm^{-1} due to C−C stretching vibration of the deoxyribose backbone,[42] suggesting that the single-stranded DNA stays in close proximity on the SRR metal surface. Other noticeable bands located at 1128 and 1237 cm^{-1} are assigned to unpaired dT (N3) residues,[7,43] and the 1274 cm^{-1} band is due to C−H deformation of thymine.[42] The strong peak observed at 1374 cm^{-1} is responsible for the virtual coincidence of a C2′-*endo/syn* dG with the C2′-*endo/anti* dT markers.[44] Especially, no Raman signal from the thiolated AS1411 was detected from a 30-nm-thick Au film on the same chip under the same conditions (black line, Figure 3B) and also from the AS1411 DNA samples without using the SRR substrate (both in solution phase and on a Si substrate; see Figure S3). Therefore, the high-quality Raman spectra are solely attributable to a typical local electromagnetic enhancement derived from the SERS effect.

When K^+ ions are introduced, dramatic changes in the Raman signal of AS1411 are observed with a sharp and strong peak centered at 1482 ± 3 cm^{-1}, which is a diagnostic marker of the C8═N7−H2 Hoogsteen hydrogen bonding of the folded G-quadruplex structure.[7,42−45] This band was not obtained in the AS1411 sample treated in water, where only weak hydrogen bonding of the guanine N7 was observed at 1492 cm^{-1} instead.[45] We also observed no Hoogsteen-type hydrogen bonding when AS1411 was incubated in Li^+ buffer or hybridized with its complementary DNA sequence (Figure S6). The G-quadruplex formation in K^+ was also confirmed by circular dichroism (CD) spectroscopy (Figure S7), and the K^+ buffer does not affect the final SERS spectrum of AS1411 (Figure S8). Furthermore, the C2′-*endo/syn* dG mode at 1374 cm^{-1} shifts to 1363 cm^{-1}, which is a marker band of C2′-*endo/anti* dG and is sensitive to antiparallel conformation and G-tetrad stacking.[43,44] Accompanying the strong band markers corresponding to the formations of G-tetrads and G-quadruplex, another important observation is the diminishment of the deoxyribose vibration band of the DNA backbone at 1005 cm^{-1} and its shift to 993 cm^{-1} with much lower intensity. This might be attributed to a "standing-up" orientation of the AS1411 G-quadruplex rather than the "lying-flat" configuration of the unfolded AS1411 on the SRR surface.[7] Furthermore, the U-shaped SRR metasensors can detect the reversible spectral modulations in response to the conformational changes of the AS1411 G-quadruplex. As shown in Figure 3B, the intensity of the Hoogsteen hydrogen bond deformation band at 1482 cm^{-1} is reduced when the G-quadruplex-functionalized SRRs were mildly rinsed in water. This is because the K^+ ions are slowly released, resulting in the loss of hydrogen bonding between N7 and H2 of the guanine residues and thus leading to a randomly loosening state between the G-tetrad planes. The diagnostic Hoogsteen band is completely ruptured as the functional SRRs are subsequently treated in water at 90 °C for 10 min. This observation is consistent with the increase in the intensity of the Raman band around 993−1005 cm^{-1}, corresponding to the deoxyribose vibration modes, suggesting that the DNA conformation is switched from the "standing-up" topology of the G-quadruplex to the "lying-down" or unfolded configuration of the AS1411 on the metallic SRR substrate. Other predominant Raman features of the AS1411 are also restored to their initial states after a stringent wash at 90 °C. In addition, the ER reversibly shifts back to ∼889 nm due to the disassembling of the G-quadruplex structure (Figure 3A).

After demonstrating the label-free and conformation-resolving plasmonic nanosensor by SERS, we further examine its potential for quantitative detection and identification of RGG_9 peptide. The RGG_9 peptide exhibits two predominant bands at 1038 and 1170 cm^{-1} (Figure 4A, bottom trace), which are characteristic bands of C-NH_3^+ antisymmetric stretching and −NH_3^+ wagging modes, respectively.[46] Upon binding to the AS1411 G-quadruplex immobilized on the SRR surface to form G-quadruplex-RGG_9 complexes, the resulting Raman spectrum exhibits the fingerprinting bands of RGG_9 at 1038 and 1172 cm^{-1} (Figure 4A, upper trace). A few Raman bands increase significantly, which can be assigned to the vibrational modes of the RGG_9 peptide, such as the amide III vibration at 1220 cm^{-1} [6] and the $C_{\alpha 2}H_2$ wagging vibration at 1303 cm^{-1}.[46] Such enhancement is probably caused by the different conformational arrangement of molecules with respect to the metal surface upon binding, leading to a stronger SERS effect. The intense Hoogsteen hydrogen band located at 1485 cm^{-1} in the upper trace indicates that the G-quadruplex structure is maintained after the binding.

Quantitative analysis and determination of binding affinity have been done by incubating various 10-fold dilutions of the RGG_9 peptide ranging from 0 to 10^{-5} M with the AS1411 G-quadruplex attached on U45 SRRs. Figure 4B shows typical transmission spectra of the metasensor *versus* RGG_9 concentrations, where the ER λ_{max} shifts to the lower frequency regime with increasing

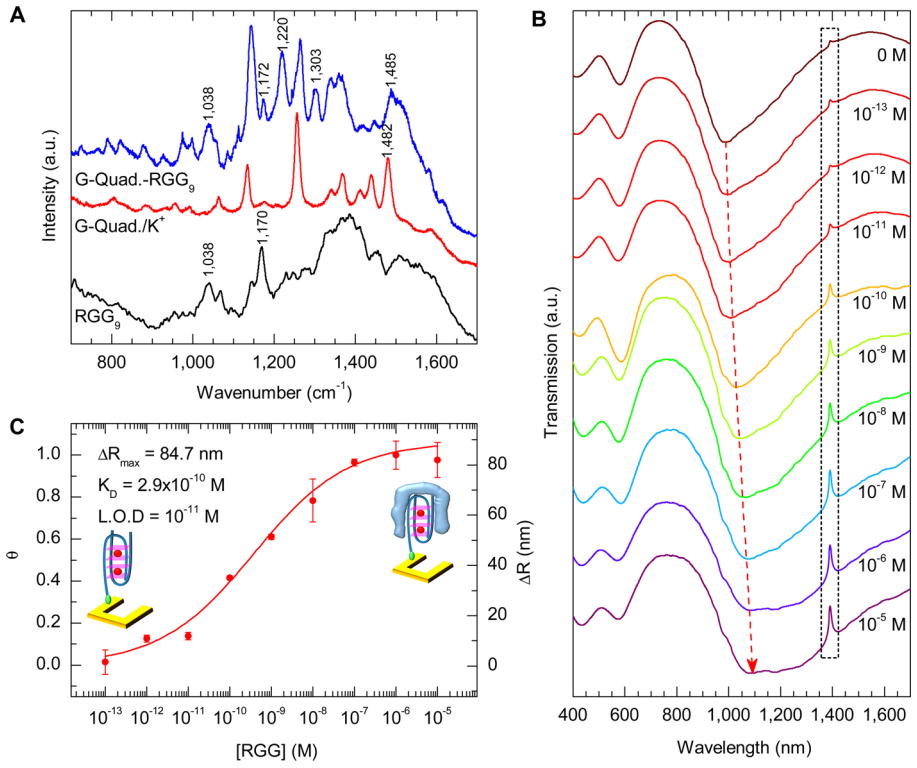

Figure 4. Detection of RGG_9 binding domain of the nucleolin cancer biomarker using the vis−NIR SRR nanosensor. (A) Raman scattering spectroscopy using the U45 SRR nanosensor for the fingerprint identification and detection of the RGG_9 binding domain of the nucleolin cancer biomarker. (B) Representative transmission spectra of vis−IR metamaterials for the detection of the RGG_9 binding domain of the nucleolin cancer biomarker at various 10-fold-diluted concentrations. The dashed rectangle marks the spectral artifact region caused by the microspectrophotometer. (C) Normalized relation of either fractional coverage values of the RGG_9 molecule ($\theta = \Delta R/\Delta R_{max}$) or ΔR as a function of RGG_9 concentration. Three different sets of U45 SRRs were used.

concentration of RGG_9. The highest wavelength shift ΔR_{max} (where $\Delta R = \lambda_{max}$(after binding) $- \lambda_{max}$(before binding)) was found to be ~85 nm, corresponding to the surface-saturated RGG_9 concentration of 10^{-6} M. Three different sets of the U45 SRR have been investigated, and the dose response was observed with a reasonable coefficient of variation (less than 12%) across the devices. Figure 4C illustrates the normalized relation of fractional coverage values of the RGG_9 molecule (θ) or ΔR as a function of RGG_9 concentrations. With an assumption that the binding of RGG_9 and AS1411 G-quadruplex is a 1:1 interaction, the experimental data points were then fit (red sigmoidal curve) according to the Hill−Langmuir binding isotherm:[32,47]

$$\theta = \frac{\Delta R}{\Delta R_{max}} = \frac{[RGG_9]}{K_D + [RGG_9]}$$

From this fitting, the equilibrium dissociation constant (K_D) for the RGG_9−AS1411 G-quadruplex interaction is obtained as 2.9×10^{-10} M, which is comparable to the value reported in the literature.[25] The high binding affinity is benefited from a stable G-quadruplex structure of AS1411,[24] it supports as evidence that nucleolin is the primary molecular target of AS1411 G-quadruplex *in vivo*,[26] and such binding will not readily dissociate at physiological conditions. Because of this, the RGG_9 peptide could be detected with concentrations spanning from the lowest detectable concentration of 10^{-11} M to 10^{-6} M (5 orders of magnitude), in which the detection limit is ~100-fold lower and the dynamic range is much broader than the traditional gel mobility shift assay.[25]

By enabling subwavelength light localization and strong electromagnetic field enhancement, LSPR biosensors have opened up a new realm of possibilities for a broad range of chemical and biological sensing applications. Although significant progress has been made, fundamental and practical challenges still remain to be addressed. For instance, the LSPR is a nonselective sensing platform; the lack of molecular specificity has limited their use as tools for providing information regarding conformation or chemical fingerprinting of biomolecules.[3] Furthermore, conventional LSPR relies on either colloidal metallic nanoparticles or nanopatterned arrays of simple geometries.[3,4,30−32,48−50] Although the plasmon-enhanced absorbance and local electromagnetic fields of the LSPR substrates have been used for SERS,[3,7] the functionality and reproducibility of the sensors are limited because of weak plasmonic resonances, spectral broadening, or uncontrollability of the hot spot's intensity and distribution. In the case of silver film over a nanosphere (AgFON) that has previously

described LSPR and SERS substrates,[33,34] the thickness of the deposited silver layer (~200 nm) prevents the AgFON substrate from being optically transparent; therefore the substrate is not highly compatible with functionalities such as microfluidics or transparency requirements. Unlike other conventional LSPR materials, the SRR metamaterials demonstrated in this paper possess not only the electric response due to the collectively charged oscillation of the free conduction electrons within nanometer-sized metallic structure but also the artificial magnetic response caused by the molecular loop current when the electric polarization is along the gap-bearing side of SRRs. The magnetic response is even more sensitive to changes in dielectric surrounding than the electric resonance that promises a sensitivity boost in LSPR-based assays. Furthermore, using electron beam lithography, the optically active multimodal SRR metamaterials could be fabricated on transparent substrates with controllable electromagnetic hot spots, high periodicity, reproducible electric field enhancement, high tunability, and less geometry variation from chip to chip (see Figure S9 for reproducible SERS signals of AS1411 immobilized on the U45 SRRs). These features are ideal for LSPR and SERS measurements and could not be achieved by those using aggregations of metallic nanoparticles.

In addition to the AS1411, there are many other GROs that may have a similar or better antiproliferative effect upon binding to nucleolin;[26] however their functions and mechanisms have not yet been studied systematically. The vis–NIR metamaterials demonstrated in this study therefore could be a versatile and powerful tool for not only the characterizations of conformational states and functions of the existing GROs for rational design of new anticancer drugs with better chemotherapeutic efficiency but also the label-free affinity binding analysis and detection of cancer biomarkers with high sensitivity.

CONCLUSION

In conclusion, we have successfully demonstrated the artificial tunable SRR metamaterials as dual transducing mode nanosensors for resolving characteristic vibrational fingerprints and conformational states of the G-quadruplex and for quantifying the aptamer–peptide binding affinity. With unprecedented spatial and structural resolution the SRR metamaterials will enable new exciting capabilities for reliable, reproducible, and label-free analysis that could be implemented in fundamental research of conformational dynamics and molecular interactions of biomolecules (ligand–receptor, DNA–DNA, DNA–protein, *etc.*). Furthermore, the fabrication of metamaterials is compatible with microfluidics and microsystems, enabling the transition of advances in plasmonic materials into fully integrated and miniaturized microdevices with huge potential applications in discovery of new drugs and disease diagnosis.

METHODS

Biological Materials and Reagents. Purified oligonucleotides AS1411 (5′-GGT GGT GGT GGT TGT GGT GGT GGT GG-3′), thiolated AS1411 (5′ thiol modifier C6 S-S-GGT GGT GGT GGT TGT GGT GGT GGT GG-3′), and a complementary sequence of AS1411 (5′- CCA CCA CCA CCA CAA CCA CCA CCA CC-3′) were purchased from Integrated DNA Technologies, Singapore. RGG_9 peptide (41 amino acids, 3.7 kDa) was obtained from SBS General Store, Nanyang Technological University, Singapore. NAP-5 columns were purchased from GE Healthcare, Singapore. Dithiothreitol (DTT) and other essential chemicals were of analytical grade and obtained from Sigma-Aldrich, Singapore, unless otherwise stated. All experiments were done using DNA-free water (1st Base, Singapore).

Fabrication of U-Shaped SRR-Based Plasmonic Substrate. The U-shaped SRRs with different line widths of 35, 45, and 55 nm were fabricated on 0.7-mm-thick ITO glass over an area of 40 μm × 40 μm by electron beam lithography. Commercial electron beam resist polymethyl methacrylate (950 PMMA A 4, MicroChem, USA) was spin-coated at 4000 rpm for 1 min on ITO glass and baked at 180 °C for 20 min. The designed structures (geometrical parameters and periodicity of the unit cell are described in the SI, Figure S1) were written using a JEOL 7001F SEM equipped with a nanometer pattern generation system and then developed in 1:3 methyl isobutyl ketone/isopropyl alcohol developer (MicroChem, USA) for 90 s. After the development, a 30 nm Au film with 2 nm of Cr as an adhesive layer was deposited using thermal evaporation deposition (Elite Engineering, Singapore) at a base pressure of 3×10^{-7} Torr. Finally, the sample was immersed in acetone for at least 3 h for lift-off and washed thoroughly with isopropyl alcohol and water.

Preparation of DNA-Functionalized SRR-Based Nanosensors. The 100 μM thiolated AS1411 was first mixed with 150 mM dithiothreitol at room temperature for 2 h to deprotect the terminal thiol group. After the deprotection, the thiolated AS1411 was desalted and purified using a NAP-5 column. Then 0.4 μL of freshly deprotected thiolated AS1411 oligonucleotides (10 μM) was spotted on clean Au SRR samples and incubated overnight in a humid chamber to avoid evaporation. The samples were subsequently washed with DNA-free water to remove any unbound DNA.

Analysis of G-Quadruplex Formation. The thiolated AS1411 DNA immobilized on the SRRs was studied in different solutions: DNA-free water, K^+ buffer (50 mM HEPES buffer pH 7.4, 40 mM KCl, 400 mM NaCl, 0.1% Triton X-100, 2% dimethyl sulfoxide), and Li^+ buffer (90 mM LiCl, 30 mM H_3PO_4, pH 7.1). The samples were heated to 90 °C for 10 min and then slowly cooled to room temperature for 8 h in the presence of 10 μM AS1411 to allow any potential GROs to form G-quadruplex structures. Formation of a duplex structure was also performed by hybridizing the immobilized AS1411 with its complementary sequence in 50 mM HEPES buffer (pH 7.4). The samples were then mildly washed by the corresponding buffers, dried with nitrogen gas, and then measured by transmission and SERS spectroscopies.

Detection of RGG_9 Binding Domain of Nucleolin Cancer Biomarker Using Vis–NIR SRR Metamaterials. The U45 SRRs attached with the K^+-induced AS1411 G-quadruplexes were used as plasmonic nanosensors for the detection of RGG_9 peptide. The RGG_9 peptide was prepared in 25 mM HEPES buffer (pH 7.4) containing 10 mM KCl, 100 mM NaCl, and 0.05% Triton X-100. Subsequently, 0.4 μL of various 10-fold dilutions of the RGG_9 peptide (10^0–10^{-5} M) was incubated with the functionalized nanosensors in a humid chamber at room temperature for 2 h. The nanosensors were then washed by the HEPES buffer, dried with nitrogen gas, and then measured by transmission and SERS spectroscopies.

Transmission and SERS Measurements. The transmission spectra on the SRR substrates were collected using a microspectrometer (Craic 20) in the range 400–1700 nm. The Raman scattering

spectroscopy was performed on the SRR substrates using a micro-Raman spectrometer (Horiba-JY T64000) excited with a diode laser (λ = 785 nm) in the backscattering configuration. The backscattered signal was collected through a 50× objective lens and dispersed by a 1800 g/mm grating. The laser power on the sample surface was measured at about 3 mW; acquisition time was 100 s.

Simulation. The electromagnetic field of the metamaterials is simulated by the discrete dipole approximation method using the DDSCAT program (version 7.1),[35−37] and 2 nm grids were used for all simulations. The average and maximum electric field intensities over the nanoparticle surface were calculated for isolated metamolecules in a homogeneous dielectric environment where the substrate effect was included explicitly by effective media theory. The data were used to produce contour plots of the intensity on and around the nanoparticle to visualize the location of the hot spots. The transmission curves of metamaterials with different sizes are computed based on a finite difference time-domain open source MEEP code.

Conflict of Interest: The authors declare no competing financial interest.

Acknowledgment. The author Q.X. thanks the strong support from Singapore National Research Foundation through a Fellowship grant (NRF-RF2009-06) and very strong support from Nanyang Technological University *via* a start-up grant (M58110061). Q.X. and S.L. gratefully acknowledge the support from Singapore Ministry of Education *via* a Tier 2 grant (MOE2011-T2-2-085(ARC 12/12)).

Supporting Information Available: Geometrical parameters and periodicity of the unit cell (Figure S1); sensitivity factors of three different unit sizes of U-shaped SRRs (Figure S2); Raman spectra of AS1411 measured in solution phase and dry state (Figure S3); calculation of enhancement factor *via* 2-naphthalenethiol (Figure S4); examination of RI effect caused by K^+ washing buffer (Figure S5); SERS spectra of AS1411 as treated in Li^+ and hybridized with complementary DNA sequence (Figure S6); CD spectra of SH-AS1411 in water and in K^+ buffer (Figure S7); examination of K^+ buffer affecting the SERS signal generated by U45 SRRs (Figure S8); and Raman scattering spectroscopy of the unfolded AS1411 immoblized on U45 SRRs (Figure S9). This material is available free of charge *via* the Internet at http://pubs.acs.org.

REFERENCES AND NOTES

1. Dobson, C. Protein Folding and Misfolding. *Nature* **2003**, *426*, 884–890.
2. Liedberg, B.; Nylander, C.; Lundstrom, I. Surface-Plasmon Resonance for Gas-Detection and Biosensing. *Sens. Actuators* **1983**, *4*, 299–304.
3. Anker, J. N.; Hall, W. P.; Lyandres, O.; Shah, N. C.; Zhao, J.; Van Duyne, R. P. Biosensing with Plasmonic Nanosensors. *Nat. Mater.* **2008**, *7*, 442–453.
4. Hall, W. P.; Modica, J.; Anker, J.; Lin, Y.; Mrksich, M.; Van Duyne, R. P. A Conformation- and Ion-Sensitive Plasmonic Biosensor. *Nano Lett.* **2011**, *11*, 1098–1105.
5. Sherry, L. J.; Jin, R.; Mirkin, C. A.; Schatz, G. C.; Van Duyne, R. P. Localized Surface Plasmon Resonance Spectroscopy of Single Silver Triangular Nanoprisms. *Nano Lett.* **2006**, *6*, 2060–2065.
6. Ochsenkuehn, M. A.; Campbell, C. J. Probing Biomolecular Interactions Using Surface Enhanced Raman Spectroscopy: Label-Free Protein Detection Using a G-Quadruplex DNA Aptamer. *Chem. Commun.* **2010**, *46*, 2799–2801.
7. Rusciano, G.; De Luca, A. C.; Pesce, G.; Sasso, A.; Oliviero, G.; Amato, J.; Borbone, N.; D'Errico, S.; Piccialli, V.; Piccialli, G.; *et al*. Label-Free Probing of G-Quadruplex Formation by Surface-Enhanced Raman Scattering. *Anal. Chem.* **2011**, *83*, 6849–6855.
8. Lim, D.; Jeon, K.; Hwang, J.; Kim, H.; Kwon, S.; Suh, Y. D.; Nam, J. Highly Uniform and Reproducible Surface-Enhanced Raman Scattering from DNA-Tailorable Nanoparticles with 1-nm Interior Gap. *Nat. Nanotechnol.* **2011**, *6*, 452–460.
9. Ko, H.; Singamaneni, S.; Tsukruk, V. V. Nanostructured Surfaces and Assemblies as SERS Media. *Small* **2008**, *4*, 1576–1599.
10. Clark, A. W.; Glidle, A.; Cumming, D. R. S.; Cooper, J. M. Plasmonic Split-Ring Resonators as Dichroic Nanophotonic DNA Biosensors. *J. Am. Chem. Soc.* **2009**, *131*, 17615–17619.
11. Hendry, E.; Carpy, T.; Johnston, J.; Popland, M.; Mikhaylovskiy, R. V.; Lapthorn, A. J.; Kelly, S. M.; Barron, L. D.; Gadegaard, N.; Kadodwala, M. Ultrasensitive Detection and Characterization of Biomolecules Using Superchiral Fields. *Nat. Nanotechnol.* **2010**, *5*, 783–787.
12. Kabashin, A. V.; Evans, P.; Pastkovsky, S.; Hendren, W.; Wurtz, G. A.; Atkinson, R.; Pollard, R.; Podolskiy, V. A.; Zayats, A. V. Plasmonic Nanorod Metamaterials for Biosensing. *Nat. Mater.* **2009**, *8*, 867–871.
13. Pryce, I. M.; Kelaita, Y. A.; Aydin, K.; Atwater, H. A. Compliant Metamaterials for Resonantly Enhanced Infrared Absorption Spectroscopy and Refractive Index Sensing. *ACS Nano* **2011**, *5*, 8167–8174.
14. Wu, C.; Khanikaev, A. B.; Adato, R.; Arju, N.; Yanik, A. A.; Altug, H.; Shvets, G. Fano-Resonant Asymmetric Metamaterials for Ultrasensitive Spectroscopy and Identification of Molecular Monolayers. *Nat. Mater.* **2012**, *11*, 69–75.
15. Smith, D.; Padilla, W.; Vier, D.; Nemat-Nasser, S.; Schultz, S. Composite Medium with Simultaneously Negative Permeability and Permittivity. *Phys. Rev. Lett.* **2000**, *84*, 4184–4187.
16. Shelby, R.; Smith, D.; Schultz, S. Experimental Verification of a Negative Index of Refraction. *Science* **2001**, *292*, 77–79.
17. Zheludev, N. I. The Road Ahead for Metamaterials. *Science* **2010**, *328*, 582–583.
18. Linden, S.; Enkrich, C.; Wegener, M.; Zhou, J.; Koschny, T.; Soukoulis, C. Magnetic Response of Metamaterials at 100 Terahertz. *Science* **2004**, *306*, 1351–1353.
19. Xu, X.; Peng, B.; Li, D.; Zhang, J.; Wong, L. M.; Zhang, Q.; Wang, S.; Xiong, Q. Flexible Visible-Infrared Metamaterials and Their Applications in Highly Sensitive Chemical and Biological Sensing. *Nano Lett.* **2011**, *11*, 3232–3238.
20. Soukoulis, C. M.; Linden, S.; Wegener, M. Negative Refractive Index at Optical Wavelengths. *Science* **2007**, *315*, 47–49.
21. Cubukcu, E.; Zhang, S.; Park, Y.; Bartal, G.; Zhang, X. Split Ring Resonator Sensors for infrared Detection of Single Molecular Monolayers. *Appl. Phys. Lett.* **2009**, *95*, 043113(1)–043113(3).
22. Adato, R.; Yanik, A. A.; Amsden, J. J.; Kaplan, D. L.; Omenetto, F. G.; Hong, M. K.; Erramilli, S.; Altug, H. Ultra-Sensitive Vibrational Spectroscopy of Protein Monolayers with Plasmonic Nanoantenna Arrays. *Proc. Natl. Acad. Sci. U.S.A.* **2009**, *106*, 19227–19232.
23. Girvan, A. C.; Teng, Y.; Casson, L. K.; Thomas, S. D.; Juliger, S.; Ball, M. W.; Klein, J. B.; Pierce, W. M., Jr.; Barve, S. S.; Bates, P. J. AGRO100 Inhibits Activation of Nuclear Factor-Kappa B (NF-Kappa B) by Forming a Complex with NF-Kappa B Essential Modulator (NEMO) and Nucleolin. *Mol. Cancer Ther.* **2006**, *5*, 1790–1799.
24. Soundararajan, S.; Wang, L.; Sridharan, V.; Chen, W.; Courtenay-Luck, N.; Jones, D.; Spicer, E. K.; Fernandes, D. J. Plasma Membrane Nucleolin Is a Receptor for the Anticancer Aptamer AS1411 in MV4-11 Leukemia Cells. *Mol. Pharmacol.* **2009**, *76*, 984–991.
25. Hanakahi, L.; Sun, H.; Maizels, N. High Affinity Interactions of Nucleolin with G-G-Paired rDNA. *J. Biol. Chem.* **1999**, *274*, 15908–15912.
26. Bates, P. J.; Laber, D. A.; Miller, D. M.; Thomas, S. D.; Trent, J. O. Discovery and Development of the G-Rich Oligonucleotide AS1411 as a Novel Treatment for Cancer. *Exp. Mol. Pathol.* **2009**, *86*, 151–164.
27. Yen, T.; Padilla, W.; Fang, N.; Vier, D.; Smith, D.; Pendry, J.; Basov, D.; Zhang, X. Terahertz Magnetic Response from Artificial Materials. *Science* **2004**, *303*, 1494–1496.
28. Enkrich, C.; Wegener, M.; Linden, S.; Burger, S.; Zschiedrich, L.; Schmidt, F.; Zhou, J.; Koschny, T.; Soukoulis, C. Magnetic Metamaterials at Telecommunication and Visible Frequencies. *Phys. Rev. Lett.* **2005**, *95*, 203901(1)–203901(4).

29. Oskooi, A. F.; Roundy, D.; Ibanescu, M.; Bermel, P.; Joannopoulos, J. D.; Johnson, S. G. MEEP: A Flexible Free-Software Package for Electromagnetic Simulations by the FDTD Method. *Comput. Phys. Commun.* **2010**, *181*, 687–702.
30. Haes, A.; Zou, S.; Schatz, G.; Van Duyne, R. Nanoscale Optical Biosensor: Short Range Distance Dependence of the Localized Surface Plasmon Resonance of Noble Metal Nanoparticles. *J. Phys. Chem. B* **2004**, *108*, 6961–6968.
31. Haes, A.; Van Duyne, R. A Unified View of Propagating and Localized Surface Plasmon Resonance Biosensors. *Anal. Bioanal. Chem.* **2004**, *379*, 920–930.
32. Haes, A.; Van Duyne, R. A Nanoscale Optical Blosensor: Sensitivity and Selectivity of an Approach Based on the Localized Surface Plasmon Resonance Spectroscopy of Triangular Silver Nanoparticles. *J. Am. Chem. Soc.* **2002**, *124*, 10596–10604.
33. Zhang, X.; Zhao, J.; Whitney, A. V.; Elam, J. W.; Van Duyne, R. P. Ultrastable Substrates for Surface-Enhanced Raman Spectroscopy: Al_2O_3 Overlayers Fabricated by Atomic Layer Deposition Yield Improved Anthrax Biomarker Detection. *J. Am. Chem. Soc.* **2006**, *128*, 10304–10309.
34. Zhang, X.; Young, M.; Lyandres, O.; Van Duyne, R. Rapid Detection of an Anthrax Biomarker by Surface-Enhanced Raman Spectroscopy. *J. Am. Chem. Soc.* **2005**, *127*, 4484–4489.
35. Draine, B. The Discrete-Dipole Approximation and Its Application to Interstellar Graphite Grains. *Astrophys. J.* **1988**, *333*, 848–872.
36. Draine, B.; Flatau, P. Discrete-Dipole Approximation for Scattering Calculations. *J. Opt. Soc. Am. A* **1994**, *11*, 1491–1499.
37. Draine, B.; Flatau, P. User Guide for the Discrete Dipole Approximation Code Ddscat 7.0s, http://arxiv.Org/abs/0809.0337v5, 2009.
38. Alvarez-Puebla, R.; Dos Santos, D.; Aroca, R. Surface-Enhanced Raman Scattering for Ultrasensitive Chemical Analysis of 1 and 2-Naphthalenethiols. *Analyst* **2004**, *129*, 1251–1256.
39. Ye, W.; Chen, Y.; Zhou, F.; Wang, C.; Li, Y. Fluoride-Assisted Galvanic Replacement Synthesis of Ag and Au Dendrites on Aluminum Foil with Enhanced SERS and Catalytic Activities. *J. Mater. Chem.* **2012**, *22*, 18327–18334.
40. Fu, C. Y.; Kho, K. W.; Dinish, U. S.; Koh, Z. Y.; Malini, O. Enhancement in SERS Intensity with Hierarchical Nanostructures by Bimetallic Deposition Approach. *J. Raman Spectrosc.* **2012**, *43*, 977–985.
41. Hall, W. P.; Anker, J. N.; Lin, Y.; Modica, J.; Mrksich, M.; Van Duyne, R. P. A Calcium-Modulated Plasmonic Switch. *J. Am. Chem. Soc.* **2008**, *130*, 5836–5837.
42. Pagba, C. V.; Lane, S. M.; Wachsmann-Hogiu, S. Conformational Changes in Quadruplex Oligonucleotide Structures Probed by Raman Spectroscopy. *Biomed. Opt. Express* **2011**, *2*, 207–217.
43. Wei, C.; Jia, G.; Yuan, J.; Feng, Z.; Li, C. A Spectroscopic Study on The Interactions of Porphyrin with G-Quadruplex DNAs. *Biochemistry* **2006**, *45*, 6681–6691.
44. Krafft, C.; Benevides, J.; Thomas, G. Secondary Structure Polymorphism in *Oxytricha nova* Telomeric DNA. *Nucleic Acids Res.* **2002**, *30*, 3981–3991.
45. Miura, T.; Thomas, G. Structural Polymorphism of Telomere DNA - Interquadruplex and Duplex-Quadruplex Conversions Probed by Raman-Spectroscopy. *Biochemistry* **1994**, *33*, 7848–7856.
46. Podstawka, E.; Ozaki, Y.; Proniewicz, L. Part III: Surface-Enhanced Raman Scattering of Amino Acids and Their Homodipeptide Monolayers Deposited onto Colloidal Gold Surface. *Appl. Spectrosc.* **2005**, *59*, 1516–1526.
47. Langmuir, I. The Constitution and Fundamental Properties of Solids and Liquids Part I Solids. *J. Am. Chem. Soc.* **1916**, *38*, 2221–2295.
48. Cao, C.; Sim, S. J. Resonant Rayleigh Light Scattering Response of Individual Au Nanoparticles to Antigen-Antibody Interaction. *Lab Chip* **2009**, *9*, 1836–1839.
49. Cao, C.; Li, X.; Lee, J.; Sim, S. J. Homogenous Growth of Gold Nanocrystals for Quantification of PSA Protein Biomarker. *Biosens. Bioelectron.* **2009**, *24*, 1292–1297.
50. Truong, P. L.; Cao, C.; Park, S.; Kim, M.; Sim, S. J. A New Method for Non-Labeling Attomolar Detection of Diseases Based on an Individual Gold Nanorod Immunosensor. *Lab Chip* **2011**, *11*, 2591–2597.